PAPER

Check for updates

Effects of bromine-containing counterion salts in directing the structures of medium-sized silver nanoclusters†

Haoqi Li, Xiao Wei, Xi Kang ⓘ * and Manzhou Zhu ⓘ

The preparation and structural determination of silver nanoclusters (especially the medium-sized Ag clusters) remain more challenging relative to those of their gold counterparts because of the comparative instability of the former. In this work, three medium-sized Ag clusters were controllably synthesized and structurally determined, namely, $[Ag_{52}(S\text{-}Adm)_{30}Br_4H_{20}]^{2-}$ (Ag_{52} for short), $Ag_{54}(S\text{-}Adm)_{30}Br_4H_{20}$ (Ag_{54} for short), and $[Ag_{58}(S\text{-}Adm)_{30}Br_4(NO_3)_2H_{22}]^{2+}$ (Ag_{58} for short) nanoclusters. Specifically, the introduction of PPh_4Br gave rise to the generation of Ag_{52} and Ag_{54} nanoclusters with homologous compositions and configurations, while the $TOABr$ salt selected Ag_{58} as the sole cluster product, whose geometric structure was completely different from those of Ag_{52} and Ag_{54} nanoclusters. In addition, the optical absorptions and emissions of the three medium-sized silver nanoclusters were compared. The findings in this work not only provide three uniquely medium-sized nanoclusters to enrich the silver cluster family but also point out a new approach (*i.e.*, changing the counterion salt) for the preparation of new nanoclusters with novel structures.

Department of Chemistry and Centre for Atomic Engineering of Advanced Materials, Key Laboratory of Structure and Functional Regulation of Hybrid Materials of Ministry of Education, Institutes of Physical Science and Information Technology and Anhui Province Key Laboratory of Chemistry for Inorganic/Organic Hybrid Functionalized Materials, Anhui University, Hefei, Anhui 230601, China. E-mail: kangxi_chem@ahu.edu.cn
†Electronic supplementary information (ESI) available: Fig. S1–S18 and Tables S1–S3 for the structure comparison, and ESI-MS, XPS, and NMR results of nanoclusters. CCDC 2301180, 2301182 and 2301183. For ESI and crystallographic data in CIF or other electronic format see DOI: https://doi.org/10.1039/d3nr05464k
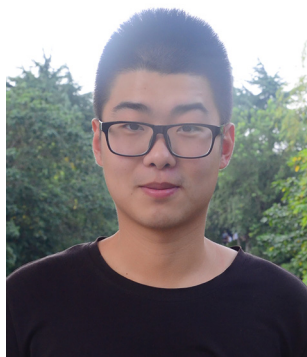
Xi Kang obtained his PhD in Chemistry from Anhui University in 2020 under the supervision of Prof. Manzhou Zhu. He is currently a Professor of Chemistry at Anhui University. His research interests include atomically precise nanoclusters and cluster-based nanomaterials.

Xi Kang

Introduction

As a special kind of metal nanomaterial, atomically precise metal nanoclusters, whose sizes are between those of metallic complexes and those of bulk metals, have attracted widespread attention in the past few decades.[1–3] Owing to the strong quantum size effect and discrete electronic energy levels, metal nanoclusters or cluster-based nanomaterials exhibit structure-dependent performances, such as optical,[4–9] electrical,[10–13] magnetic, *etc.*[14–17] Besides, the atomic precision characterization of metal nanoclusters makes them ideal nano-platforms for investigating the structural evolution mechanisms of metal-based nanostructures and the related structure–property correlations, which could, in turn, act as guidelines for the preparation of metal clusters with customized structures and tailored properties. In this context, how to control the size/structure of nanoclusters and regulate their chemical environment to obtain functional nanoclusters has aroused in-depth research interests of nanocluster scientists.[18–23]

Compared with the rich family of gold nanoclusters, there are relatively few structures on the atomically precise silver counterparts. Indeed, the comparative instability of silver nanoclusters relative to gold ones makes their preparation and isolation more challenging. To date, several silver nanoclusters with different core sizes have been prepared and structurally determined by means of one-pot synthesis, ligand engineer-

ing, intercluster assembly, *etc.*[24–35] Several of these reported silver nanoclusters comprise small-sized metallic kernels (*e.g.*, $Ag_{14–16}$,[36–38] $Ag_{20–23}$,[39–41] Ag_{25},[42] Ag_{29},[43] *etc.*) or large-sized metallic kernels (*e.g.*, Ag_{100},[44] Ag_{136},[45] Ag_{141},[46] Ag_{146},[47] Ag_{152},[48] Ag_{206},[49] $Ag_{210–211}$,[50] Ag_{307},[51] Ag_{374},[52] *etc.*). In comparison, there are fewer reports about structurally determined silver nanoclusters with medium-sized metallic kernels (*i.e.*, 50–100-atom silver kernels), which partly restrict the formation of a rich family of silver nanoclusters. Besides, ligand engineering has been developed as a versatile approach for the synthesis of silver nanoclusters with novel structures and functionalities, and the ligand effect has been evaluated in such preparations. However, most of these works focused on the thiol or phosphine ligand effects in directing the structures of metal nanoclusters. As the halide-containing salts have been widely exploited for the preparation of silver nanoclusters *via* forming Ag–halide interactions, more efforts are needed to evaluate the effect of halide-containing counterion salts in the corresponding preparations and structure formations.

In the current work, the effect of bromine-containing salts in directing the structures of silver nanoclusters was investigated, and three clusters with medium-sized metallic kernels were controllably synthesized and structurally determined. Specifically, the introduction of PPh_4Br gave rise to the generation of $[Ag_{52}(S-Adm)_{30}Br_4H_{20}]^{2-}$ (Ag_{52} for short) and $Ag_{54}(S-Adm)_{30}Br_4H_{20}$ (Ag_{54} for short) nanoclusters, while TOABr selected the $[Ag_{58}(S-Adm)_{30}Br_4(NO_3)_2H_{22}]^{2+}$ (Ag_{58} for short) nanocluster, where S-Adm is 1-adamantane thiol and TOABr is tetraoctylammonium bromide. The atomically precise structures of the three silver nanoclusters were determined by single-crystal X-ray diffraction (SC-XRD) and further confirmed by electrospray ionization mass spectrometry (ESI-MS) and nuclear magnetic resonance (NMR) measurements. The Ag_{52} and Ag_{54} nanoclusters were structurally homologous in terms of the kernel structures and the overall configurations, while the Ag_{58} nanocluster exhibited a completely different geometric structure. In addition, the optical performances, including optical absorptions and emissions, of the three silver nanoclusters were compared.

Results and discussion

The three medium-sized Ag nanoclusters (*i.e.*, Ag_{52}, Ag_{54}, and Ag_{58}) were controllably synthesized *via* a one-pot mild-reduction method (see the ESI for more details†). The borane-*tert*-butylamine complex was exploited as the reducing agent in this work to accomplish the mild reduction of the nanoclusters. Specifically, the structurally homologous Ag_{52} and Ag_{54} nanoclusters were prepared simultaneously and distinguished in the SC-XRD process, while the Ag_{58} nanocluster was prepared separately. The critical points for directing different nanoclusters (Ag_{52} and Ag_{54}, or Ag_{58}) was the introduction of different bromine-containing counterion salts—PPh_4Br or TOABr (Fig. 1). The different cluster products might be attributed to the following two aspects: (i) the alkane chain in TOABr
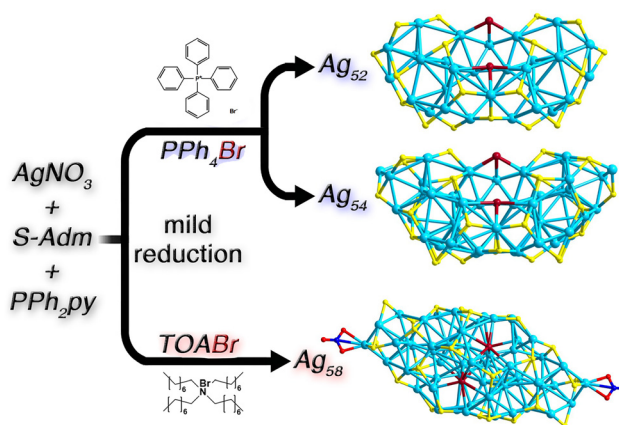

Fig. 1 Synthetic approaches of Ag_{52}, Ag_{54}, and Ag_{58} nanoclusters and their overall structures. Color labels: light blue/green = Ag; yellow = S; brown = Br; blue = N; and red = O. All C and H atoms are omitted for clarity.

was flexible, while the benzene ring in PPh_4Br was rigid. The different steric hindrances of two counterion salts resulted in distinct restriction effects in the structural rearrangement among the cluster formation process; (ii) the different interactions between counter-cations (PPh_4^+ or TOA^+) and cluster molecules would remarkably affect the final cluster formation.

The structures of Ag_{52} and Ag_{54} clusters were distinguished *via* SC-XRD (Fig. S1†). As depicted in Fig. 2, the Ag_{52} and Ag_{54} nanoclusters were highly structurally homologous in terms of their overall geometric structures. Both Ag_{52} and Ag_{54} clusters contained an Ag_{12} kernel consisting of three octahedral Ag_6 units assembled *via* an Ag_3-face-fusing pattern (Fig. 2A and B). The Ag_{12} kernel was further stabilized by four bromine ligands and seven $Ag_5(SR)_4$ motifs *via* Ag–Br and Ag–S interactions, respectively (Fig. 2C and D). The obtained $A_{46}(SR)_{28}Br_4$ structure presented the C_2 symmetry (Fig. 2D). The only difference between the geometric structures between Ag_{52} and Ag_{54} nanoclusters was their bridging motifs on two ends: two Ag linkers and two $Ag_2(SR)_1$ motifs in the Ag_{52} nanocluster, or two Ag linkers and two $Ag_3(SR)_1$ motifs in the Ag_{52} nanocluster (Fig. 2E and F). In this context, the Ag_{52} and Ag_{54} nanoclusters were highly structurally homologous with subtle differences in their terminal structures. Such similar frameworks might be the root cause for the co-generation of the two nanoclusters and the high similarity of their crystals; accordingly, the Ag_{52} and Ag_{54} clusters could only be distinguished and separated *via* SC-XRD. However, the cocrystallization of the two structure-correlated nanoclusters was not formed, which was probably due to their distinct crystal lattice energies that forced them to be crystallized into their individual crystals.[53,54] Indeed, the two nanoclusters followed different crystalline systems and space groups.

Due to their different terminal structures, Ag_{52} and Ag_{54} nanoclusters exhibited distinct bond lengths despite their homologous frameworks. Of note, the difference in peripheral structures of nanoclusters would also lead to corresponding changes in their kernel structures. For example, the octahedral
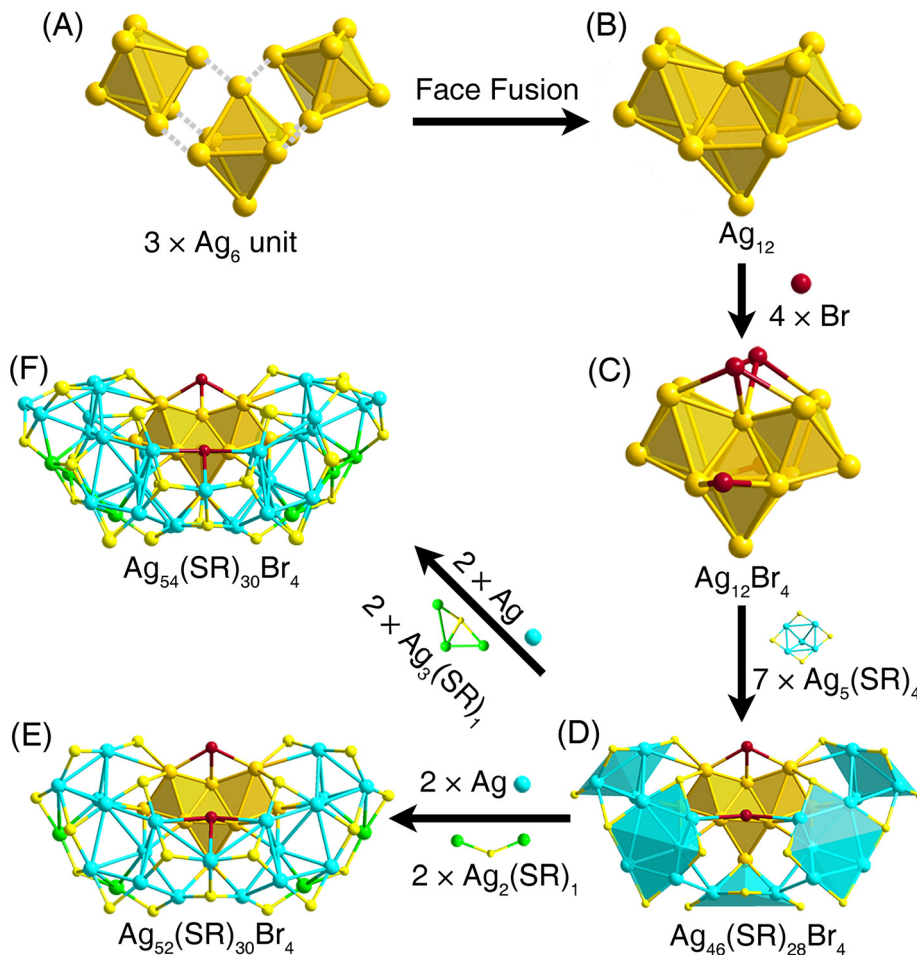
Fig. 2 Structural anatomy of Ag_{52} and Ag_{54} nanoclusters. (A) The three Ag_6 units. (B) The Ag_{12} kernel. (C) The $Ag_{12}Br_4$ kernel structure. (D) The $Ag_{46}(SR)_{28}Br_4$ structure. (E) The overall structure of $Ag_{52}(SR)_{30}Br_4$. (F) The overall structure of $Ag_{54}(SR)_{30}Br_4$. Color labels: gold/light blue/green = Ag; yellow = S; and brown = Br. All C and H atoms are omitted for clarity.

Ag_6 nuclei underwent elongation with the increasing cluster size. Specifically, the average bond length between Ag atoms in Ag_6 nuclei of Ag_{52} was 2.825 Å, which increased to 2.908 Å for Ag_{54} (Fig. S2A and S3A†). Besides, the average lengths of the Ag(core)–Ag(motif) and Ag(core)–Br bonds were shortened from 2.992 and 2.762 Å for Ag_{52} to 2.946 and 2.715 Å for Ag_{54}, respectively. In addition, both average lengths of Ag(motif)–Ag(motif) and Ag(motif)–S(motif) bonds were also reduced with the cluster size growth (Fig. S2 and S3†). The most significant structural difference between Ag_{52} and Ag_{54} was their terminal motif structures: $Ag_2(SR)_1$ in Ag_{52} and $Ag_3(SR)_1$ in Ag_{54}. Compared to the average Ag–S bond length of 2.603 Å in the $Ag_2(SR)_1$ motif of the Ag_{52} cluster, the corresponding bonds in Ag_{54} were remarkably shortened to 2.548 Å (Fig. S4†). In this context, the surface structure of Ag_{54} becomes more densely packed relative to Ag_{52} due to the incorporation of two more Ag atoms. At the same time, the kernel structure is expanded with the cluster size growth, which might result from the pulling effect of the peripheral motif frameworks of nanoclusters on their innermost kernel structures.

The introduction of the TOABr counterion that contained flexible carbon tails gave rise to the generation of the Ag_{58} nanocluster. The overall structure of Ag_{58} contained an Ag_6 core with Ag(core)–Ag(core) bond lengths ranging from 2.743 to 2.785 Å (on average, 2.770 Å). At both ends of the Ag_6 core, two polar Ag atoms (marked in blue) were symmetrically anchored onto the corresponding Ag_3 face, forming two Ag_4 tetrahedra and constituting an Ag_8 kernel (Fig. 3A and S5–S7†). The Ag_8 kernel was fixed by a ring-shaped Ag_8Br_4 motif, and four Br atoms were connected to four Ag atoms at adjacent positions on the Ag_6 core, constituting an $Ag_{16}Br_4$ structure (Fig. 3B). In contrast to the exposed Br atoms in Ag_{52} and Ag_{54}, the Br atoms in the Ag_{58} nanocluster were shielded. The average bond length of the Ag(core)–Br bonds in Ag_{58} was 2.609 Å, indicating a more compact kernel structure relative to those in Ag_{52} and Ag_{54} (Fig. S2–S4†). Furthermore, three $Ag_5(SR)_4$ motifs further stabilized the $Ag_{16}Br_4$ structure, forming an $Ag_{46}(SR)_{24}Br_4$ framework (Fig. 3C). Each three adjacent $Ag_5(SR)_4$ subunits were inter-connected *via* Ag–S interactions, forming the $Ag_{15}(SR)_{12}$ structure in a "hand in hand" manner (Fig. S6B†). Besides, each $Ag_5(SR)_4$ motif structure cor-

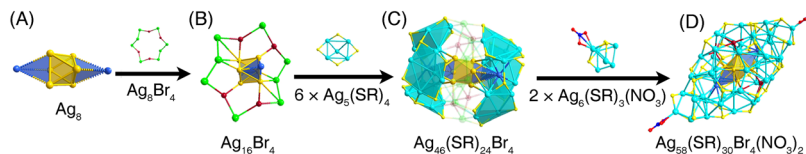**Fig. 3** Structural anatomy of the Ag_{58} nanocluster. (A) The Ag_8 kernel. (B) The $Ag_{16}Br_4$ kernel structure. (C) The $Ag_{46}(SR)_{24}Br_4$ structure. (D) The overall structure of $Ag_{58}(SR)_{30}Br_4(NO_3)_2$. Color labels: gold/light blue/green = Ag; yellow = S; brown = Br; blue = N; and red = O. All C and H atoms are omitted for clarity.

responded to the three exposed Ag_3 faces (blue faces in Fig. 3C), wherein the middle Ag atom in $Ag_5(SR)_4$ connected the polar Ag atoms at the ends of the Ag_8 kernel. Finally, two $Ag_6(SR)_3(NO_3)$ motifs were attached at both ends of the $Ag_{46}(SR)_{24}Br_4$ structure, giving rise to the overall $Ag_{58}(SR)_{30}Br_4(NO_3)_2$ structure (Fig. 3D). The average length of the Ag(core)–Ag(core) bonds in the kernel of Ag_{58} was measured at 2.770 Å, remarkably shorter than those in the Ag_{52} and Ag_{54} nanoclusters (Fig. S5A†), while the average Ag(core)–Ag(motif) bond length of Ag_{58} was much longer than those of Ag_{52} and Ag_{54} (Fig. S5B;† 3.191 Å *versus* 2.992 and 2.946 Å). In this context, the Ag_{58} nanocluster exhibited a more compact kernel structure compared to a more scattered kernel–motif shell interaction relative to the Ag_{52} and Ag_{54} nanoclusters.

Structurally, all three silver nanoclusters contained 30 thiol ligands, and the coordination modes of S (*i.e.*, the interaction modes between S and Ag) in the three nanoclusters were compared. The 30 thiol ligands in Ag_{52} and Ag_{54} exhibited three types of bonding patterns, μ_2-S, μ_3-S, and μ_4-S, by analyzing the number of Ag atoms connecting the S atom, while only μ_2-S and μ_3-S were observed in the Ag_{58} nanocluster. As the cluster size increased from Ag_{52} to Ag_{54}, the surface structure of the nanocluster became more complex with a transformation of some μ_2-S into μ_3-S (Fig. S8†). The average S–Ag coordination numbers of Ag_{52} and Ag_{54} nanoclusters were determined to be 2.324 and 2.378, respectively, demonstrating that more S–Ag interactions were generated on the Ag_{54} nanocluster surface. Moreover, a comparison of crystalline arrangement patterns was conducted (Fig. S9–S12†). The lattice symmetry of Ag_{52} (orthogonal system), Ag_{58} (monoclinic system), and Ag_{54} (triclinic system) was ordered from high to low. Accordingly, the different molecular structures of these nanoclusters could remarkably affect their supramolecular assemblies. Indeed, the supramolecular crystalline density was increased in direct proportion to the size of the nanocluster (Fig. S12†). In addition, the X-ray photoelectron spectroscopy (XPS) results of these nanoclusters demonstrated that there was no change for the Ag 3d, Br 3d, and S 2p binding energies (Fig. S13–15†), further confirming their homologous structural characterization.

The ESI-MS measurement was performed to confirm the compositions and determine the valence states of these silver nanoclusters. The mass peaks at 5484.72 and 5808.24 Da confirmed the compositions of the Ag_{52} and Ag_{58} nanoclusters

and demonstrated their valence states as $[Ag_{52}(\text{S-Adm})_{30}Br_4H_{20}]^{2-}$ and $[Ag_{58}(\text{S-Adm})_{30}Br_4H_{22}]^{2+}$, respectively (Fig. S16†). It should be noted that the two NO_3 ligands were dissociated in the ESI-MS measurement. According to the valence states of these nanoclusters, their nominal electron counts were determined as 52(Ag) − 30(SR) − 4(Br) −20(H) + 2 (charge) = 0e for $[Ag_{52}(SR)_{30}Br_4H_{20}]^{2-}$ and 58(Ag) − 30(SR) − 4(Br) − 22(H) − 2(charge) = 0e for $[Ag_{58}(SR)_{30}Br_4H_{22}]^{2+}$, demonstrating the absence of the free electron in such cluster frameworks. However, no mass signal was detected for the Ag_{54} cluster (Fig. S17†). Considering that the Ag_{52} and Ag_{54} nanoclusters shared a homologous structure, we proposed that the molecular formula for Ag_{54} should be $Ag_{54}(SR)_{30}Br_4H_{20}$. In this context, the Ag_{54} nanocluster should be electrically neutral and was difficult to ionize in the mass detection. All three silver clusters contained a large number of hydride ligands, which was rare in previously reported metal nanoclusters. However, the precise locations of such hydrides were hard to determine using an SC-XRD diffractometer due to their low electron densities. To address this issue, we attempted to replace the "H" ligands with "D" to further verify their numbers in nanoclusters by ESI-MS. However, no deuterated borane-*tert*-butylamine complex (the reducing agent in this work) was commercially available. We have tried several times to replace the reducing agent with $NaBH_4$, for which deuterated $NaBD_4$ was available; however, no cluster product was obtained since all products were decomposed after the preparation. In this context, we just employed ^1H NMR spectroscopy to confirm the presence of hydrides in the nanocluster. For the Ag_{52} nanocluster, three prominent NMR peaks at 4.67, 5.29, and 8.07 ppm were detected for the nanocluster with an area ratio of 1 : 2 : 1, while no corresponding signal was observed for the HS-Adm ligand. Consequently, it is reasonable that there are three types of hydrides within the framework of the Ag_{52} nanocluster.

The structure of clusters is the decisive factor of their physical–chemical properties. The differences in molecular structures of the three nanoclusters resulted in their distinct optical absorptions and emissions (Fig. 4). Specifically, the Ag_{52} nanocluster exhibited two distinctive absorptions at 350 and 475 nm, while Ag_{54} displayed two absorptions at 350 and 460 nm, and a shoulder band at 530 nm. In comparison, the Ag_{58} nanocluster presented two absorptions at 350 and 460 nm. Besides, the emission wavelengths of the Ag_{52}, Ag_{54}, and Ag_{58} nanoclusters were 613, 617, and 602 nm, respectively.
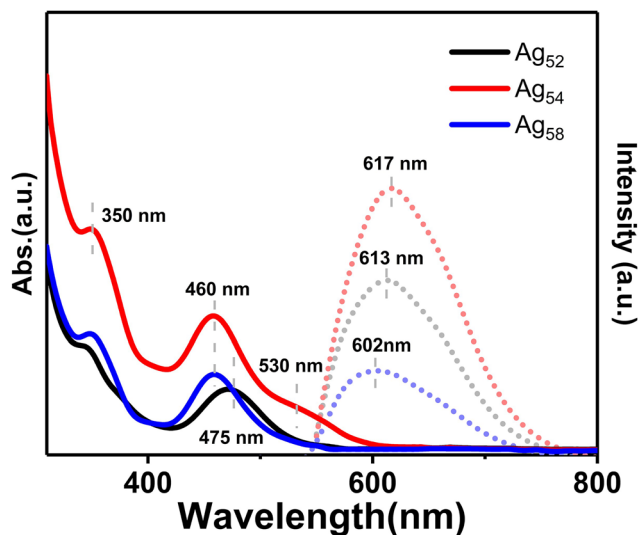
Fig. 4 Comparison of optical absorptions (solid lines) and emissions (dot lines) of Ag_{52} (black lines), Ag_{54} (red lines), and Ag_{58} (blue lines) nanoclusters (cluster molecules were dissolved in CH_2Cl_2).

In addition, compared to the Ag_{54} and Ag_{52} nanoclusters with homologous structures, the Ag_{58} nanocluster exhibited a remarkably reduced photoluminescence intensity. Besides, we found that the Ag_{54} nanocluster exhibited an enhanced PL intensity relative to its structure-related Ag_{52} nanocluster. Such an enhancement was rational by considering that the Ag_{54} nanocluster showed a more compact molecular structure, which decreased the non-radiative transition and enhanced the radiative transition (*i.e.*, the PL).[55,56]

Conclusion

In summary, three medium-sized silver nanoclusters, namely, Ag_{52}, Ag_{54}, and Ag_{58}, were controllably synthesized by adjusting the bromine-containing counterion salts in the synthetic process. Accordingly, the effects of Br-based counterion salts in directing the structures of silver nanoclusters were evaluated. Among the three nanoclusters, Ag_{52} and Ag_{54} were structurally homologous in terms of their kernel structures and overall configurations, while the configuration of the Ag_{58} nanocluster was completely different. The structure-dependent optical properties (*i.e.*, optical absorption and emission) of the three nanoclusters were evaluated. The findings in this work not only expand the structural diversity of the silver nanocluster family but also demonstrate the counterion effect in the preparation of new nanoclusters with novel structures.

Data availability

CCDC 2301180, 2301182 and 2301183 contain the supplementary crystallographic data for this paper.†

Author contributions

H. L. and X. W. performed the experiments. H. L., X. W. and X. K. wrote the manuscript. X. K. and M. Z. supervised the project. All authors commented on and agreed on the manuscript.

Conflicts of interest

There are no conflicts to declare.

Acknowledgements

References

1 E. Roduner, *Chem. Soc. Rev.*, 2006, **35**, 583.
2 R. Jin, C. Zeng, M. Zhou and Y. Chen, *Chem. Rev.*, 2016, **116**, 10346.
3 Y. Li, M. Zhou and R. Jin, *Adv. Mater.*, 2021, **33**, 2006591.
4 X. Kang and M. Zhu, *Chem. Soc. Rev.*, 2019, **48**, 2422.
5 Y. Jin, C. Zhang, X.-Y. Dong, S.-Q. Zang and T. C. W. Mak, *Chem. Soc. Rev.*, 2021, **50**, 2297.
6 W. Ishii, Y. Okayasu, Y. Kobayashi, R. Tanaka, S. Katao, Y. Nishikawa, T. Kawai and T. Nakashima, *J. Am. Chem. Soc.*, 2023, **145**, 11236.
7 Q. Li, C. J. Zeman IV, G. C. Schatz and X. W. Gu, *ACS Nano*, 2021, **15**, 16095.
8 L. Fang, W. Fan, G. Bian, R. Wang, Q. You, W. Gu, N. Xia, L. Liao, J. Li, H. Deng, N. Yan and Z. Wu, *Angew. Chem., Int. Ed.*, 2023, **62**, e202305604.
9 Y. Chen, M. Zhou, Q. Li, H. Gronlund and R. Jin, *Chem. Sci.*, 2020, **11**, 8176.
10 K. Kwak and D. Lee, *Acc. Chem. Res.*, 2019, **52**, 12.
11 X. Ouyang, Y. Wu, L. Guo, L. Li, M. Zhou, X. Li, T. Liu, Y. Ding, H. Bu, G. Xie, J. Shen, C. Fan and L. Wang, *Angew. Chem., Int. Ed.*, 2023, **62**, e202300893.
12 Y. Feng, N. Wang and H. Ju, *Sci. China: Chem.*, 2022, **65**, 2417.
13 D. Wang, X. Gao, J. Jia, B. Zhang and G. Zou, *ACS Nano*, 2023, **17**, 355.
14 J. Foxley and K. L. Knappenberger, *Annu. Rev. Phys. Chem.*, 2023, **74**, 53.
15 Y. Liu, W. Luo, Q. Fan, H. Ma, Y. Yin, Y. Long and J. Guan, *Adv. Funct. Mater.*, 2023, 2303470.
16 O. López-Estrada, B. Zuniga-Gutierrez and E. Selenius, *Nat. Commun.*, 2021, **12**, 2477.
17 Y. Li, S. Biswas, T. Luo, R. Juarez-Mosqueda, M. G. Taylor, G. Mpourmpakis, N. L. Rosi, M. P. Hendrich and R. Jin, *Chem. Mater.*, 2020, **32**, 9238.

18 R. Jin, G. Li, S. Sharma, Y. Li and X. Du, *Chem. Rev.*, 2021, **121**, 567.

19 Y. Du, H. Sheng, D. Astruc and M. Zhu, *Chem. Rev.*, 2020, **120**, 526.

20 Z. Wang, M. Du, P. Braunstein and J. Lang, *J. Am. Chem. Soc.*, 2023, **145**, 9982.

21 J.S. Kim, H. Chang, S. Kang, S. Cha, H. Cho, S.J. Kwak, N. Park, Y. Kim, D. Kang, C.K. Song, J. Kwag, J. Hahn, W. B. Lee, T. Hyeon and J. Park, *Nat. Commun.*, 2023, **14**, 3201.

22 W. Suzuki, R. Takahata, Y. Chiga, S. Kikkawa, S. Yamazoe, Y. Mizuhata, N. Tokitoh and T. Teranishi, *J. Am. Chem. Soc.*, 2022, **144**, 12310.

23 Y. Wang, B. Nieto-Ortega and T. Burgi, *Nat. Commun.*, 2020, **11**, 4562.

24 Y.-P. Xie, Y.-L. Shen, G.-X. Duan, J. Han, L.-P. Zhang and X. Lu, *Mater. Chem. Front.*, 2020, **4**, 2205.

25 S. Takano and T. Tsukuda, *J. Am. Chem. Soc.*, 2021, **143**, 1683.

26 Y. Cao, S. Malola, M. F. Matus, T. Chen, Q. Yao, R. Shi, H. Häkkinen and J. Xie, *Chem.*, 2021, **7**, 2227.

27 S. Takano and T. Tsukuda, *J. Am. Chem. Soc.*, 2021, **143**, 1683.

28 Y. Cao, S. Malola, M. F. Matus, T. Chen, Q. Yao, R. Shi, H. Häkkinen and J. Xie, *Chem.*, 2021, **7**, 2227.

29 Y. Cao, J. Guo, R. Shi, G. I. N. Waterhouse, J. Pan, Z. Du, Q. Yao, L.-Z. Wu, C.-H. Tung, J. Xie and T. Zhang, *Nat. Commun.*, 2018, **9**, 2379.

30 Y. Wang and T. Burgi, *Nanoscale Adv.*, 2021, **3**, 2710.

31 C.-Y. Liu, S.-F. Yuan, S. Wang, Z.-J. Guan, D.-E. Jiang and Q.-M. Wang, *Nat. Commun.*, 2022, **13**, 2082.

32 S. Hossain, Y. Niihori, L. V. Nair, B. Kumar, W. Kurashige and Y. Negishi, *Acc. Chem. Res.*, 2018, **51**, 3114.

33 Q. Yao, X. Yuan, T. Chen, D. T. Leong and J. Xie, *Adv. Mater.*, 2018, **30**, 1802751.

34 S. Wang, X. Meng, A. Das, T. Li, Y. Song, T. Cao, X. Zhu, M. Zhu and R. Jin, *Angew. Chem., Int. Ed.*, 2014, **53**, 2376.

35 T. Higaki, Q. Li, M. Zhou, S. Zhao, Y. Li, S. Li and R. Jin, *Acc. Chem. Res.*, 2018, **51**, 2764.

36 H. Yang, J. Lei, B. Wu, Y. Wang, M. Zhou, A. Xia, L. Zheng and N. Zheng, *Chem. Commun.*, 2013, **49**, 300.

37 X. Shen, X. Ma, Q. Ni, M. Ma, L. Gui, C. Hou, R. Hou and X. Wang, *Nanoscale*, 2018, **10**, 515.

38 H. Yang, Y. Wang and N. Zheng, *Nanoscale*, 2013, **5**, 2674.

39 W. Chang, P. Lee, J. Liao, K. K. Chakrahari, S. Kahlal, Y. Liu, M. Chiang, J. Saillard and C. W. Liu, *Angew. Chem., Int. Ed.*, 2017, **56**, 10178.

40 R. S. Dhayal, J. Liao, Y. Liu, M. Chiang, S. Kahlal, J. Saillard and C. W. Liu, *Angew. Chem., Int. Ed.*, 2015, **54**, 3702.

41 C. Liu, T. Li, H. Abroshan, Z. Li, C. Zhang, H. J. Kim, G. Li and R. Jin, *Nat. Commun.*, 2018, **9**, 744.

42 C. P. Joshi, M. S. Bootharaju, M. J. Alhilaly and O. M. Bakr, *J. Am. Chem. Soc.*, 2015, **137**, 11578.

43 L. G. AbdulHalim, M. S. Bootharaju, Q. Tang, S. D. Gobbo, R. G. AbdulHalim, M. Eddaoudi, D.-E. Jiang and O. M. Bakr, *J. Am. Chem. Soc.*, 2015, **137**, 11970.

44 X. Ma, Y. Bai, Y. Song, Q. Li, Y. Lv, H. Zhang, H. Yu and M. Zhu, *Angew. Chem., Int. Ed.*, 2020, **59**, 17234.

45 H. Yang, Y. Wang, X. Chen, X. Zhao, L. Gu, H. Huang, J. Yan, C. Xu, G. Li, J. Wu, A. J. Edwards, B. Dittrich, Z. Tang, D. Wang, L. Lehtovaara, H. Häkkinen and N. Zheng, *Nat. Commun.*, 2016, **7**, 12809.

46 L. Ren, P. Yuan, H. Su, S. Malola, S. Lin, Z. Tang, B. K. Teo, H. Häkkinen, L. Zheng and N. Zheng, *J. Am. Chem. Soc.*, 2017, **139**, 13288.

47 Y. Song, K. Lambright, M. Zhou, K. Kirschbaum, J. Xiang, A. Xia, M. Zhu and R. Jin, *ACS Nano*, 2018, **12**, 9318.

48 I. Chakraborty, A. Govindarajan, J. Erusappan, A. Ghosh, T. Pradeep, B. Yoon, R. L. Whetten and U. Landman, *Nano Lett.*, 2012, **12**, 5861.

49 L. Ren, P. Yuan, H. Su, S. Malola, S. Lin, Z. Tang, B. K. Teo, H. Häkkinen, L. Zheng and N. Zheng, *J. Am. Chem. Soc.*, 2017, **139**, 13288.

50 J. Liu, F. Alkan, Z. Wang, Z. Zhang, M. Kurmoo, Z. Yan, Q. Zhao, C. M. Aikens, C. Tung and D. Sun, *Angew. Chem., Int. Ed.*, 2019, **58**, 195.

51 M. Ma, X. Ma, G. Liang, X. Shen, Q. Ni, L. Gui, X. Wang, S. Huang and S. Li, *J. Am. Chem. Soc.*, 2021, **143**, 13731.

52 H. Yang, Y. Wang, X. Chen, X. Zhao, L. Gu, H. Huang, J. Yan, C. Xu, G. Li, J. Wu, A. J. Edwards, B. Dittrich, Z. Tang, D. Wang, L. Lehtovaara, H. Häkkinen and N. Zheng, *Nat. Commun.*, 2016, **7**, 1280.

53 X. Kang and M. Zhu, *ACS Mater. Lett.*, 2020, **2**, 1303.

54 H. Shen, X. Wei, C. Xu, S. Jin, S. Wang, X. Kang and M. Zhu, *Nanoscale*, 2021, **13**, 7694.

55 J. Xin, J. Xu, C. Zhu, Y. Tian, Q. Zhang, X. Kang and M. Zhu, *Chem. Sci.*, 2023, **14**, 8474.

56 X. Kang, S. Wang and M. Zhu, *Chem. Sci.*, 2018, **9**, 3062.